



***L*-edge photoelectron spectra of silicon hydride cations: Imprint of molecular-field and spin-orbit effects**

Alessandra Puglisi, Patricia Selles, Nicolas Sisourat , and Stéphane Carniato ^{*}
Sorbonne Université, Centre National de la Recherche Scientifique, UMR 7614,
Laboratoire de Chimie Physique–Matière et Rayonnement, 75005 Paris, France

 (Received 16 June 2020; accepted 1 September 2020; published 5 October 2020)

We study the $2p$ core hole states of the $\text{SiH}^+_{(n=1,2,3)}$ silicon hydride cations. The L -edge photoelectron spectra for these species are computed thanks to a nonperturbative effective Hamiltonian model. Furthermore, we investigate the signature on the photoelectron spectra of the relative sign and strength of the spin-orbit and molecular-field splittings. We show that, in the silicon hydride cations, the absolute values of these two contributions are of comparable magnitude but their relative signs may differ, leading to substantially different photoelectron spectra. We show that the valence shell occupation in the ground state of the systems controls the sign of the molecular-field splitting. The electronic relaxation and correlation effects on the spectra are also examined.

DOI: [10.1103/PhysRevA.102.042801](https://doi.org/10.1103/PhysRevA.102.042801)

I. INTRODUCTION

Core-level binding energies (BEs) probed by photoelectron spectroscopy or consecutive Auger electron spectroscopy provide information on the chemical environment of an atom embedded in molecular or solid-state systems. Different environments relative to the chemical bonds induce different binding energies. This major effect is the well-known chemical shift effect. However, electronic spectra obtained after a photon absorption in the x-ray domain are also highly dependent on the interplay between spin-orbit (SO) and molecular-field (MF) splittings.

The importance for core excitation of MF splitting has been known since the 1970s [1] in the d level of metallic complexes. Advances in synchrotron light sources and electron spectrometers made it possible in the 1990s to study MF splittings in spectra of core electrons deeper than typically 30 eV. Pioneering experimental studies by Bancroft and coworkers [2,3] thus revealed MF effects in I - $4d$ photoelectron (PE) spectra of iodine molecules and analyzed them using the usual crystal-field and SO Hamiltonian. They revealed a dominant noncubic component and reproduced the well-known splittings of d levels in transition metals. Previously obtained NVV ($4d^{-1} \rightarrow \pi^{-2}$) Auger electron (AE) spectra of the HI molecule [4] were then reinterpreted [5] in order to take into account the MF splittings revealed by Bancroft and coworkers [2,3]. The complementarity between PE core spectra on one side and more complex photoabsorption (PA) and AE core spectra on the other side was also illustrated for the Br- $3d$ level of the HBr molecule. MVV ($3d^{-1} \rightarrow \pi^{-2}$) AE spectra recorded earlier [6] were reassigned a few years later by Liu and coworkers [7] once the importance of MF effects had been established thanks to the analysis of Br- $3d$ PE spectra. In the

high-resolution PA spectra recorded by Püttner and coworkers [8] knowledge of MF splittings made it also possible to assign Rydberg states up to high quantum numbers.

In the 1990s the MF splittings of even deeper L -shell ($2p$) core hole states were observed in high-resolution PE spectroscopy for sulfur compounds [9–11] and for chlorinated species [12–15]. Significant variations of Auger decay rates could then be established [9] for the different MF split components. New propensity rules specifying that oriented MF split core holes decay preferentially by involving a valence orbital with the same spatial orientation were also stated [10]. These “Svensson” rules were generalized later for $3d$ core hole decay [16]. Moreover, a previous apparent ambiguity [17] between PE and AE spectra was solved and breakdown of the constant core hole lifetime broadening was demonstrated [10]. Accurate information on the splitting of core excited Rydberg states and clear identification of vibrational progressions could be obtained in high-resolution PA spectra of H_2S and D_2S molecules [18].

Interpretation of core hole spectra is a challenging task as vibrational progressions and lifetime broadenings made also a large number of MF split structures overlapping each other. It is therefore crucial to predict the contribution of the different effects. Theoretical modelings of SO interaction and MF splittings are thus greatly helpful in order to clarify the spectra and to assign the different structures.

Ab initio quantum descriptions of MF splittings in $2p$ core hole PE spectra were proposed in the 1990s by Børve and coworkers [11,19]. They demonstrated that the splittings observed in S- $2p$ PE spectra could be reproduced by an effective Hamiltonian (EH) built on nonrelativistic binding energies of the core hole states and SO interaction in the $2p$ level. Standard fully relativistic simulations were also implemented in order to assign the $2p$ core hole PE spectra for the HCl molecule [20]. Unfortunately the signature of MF effects is tenuous in S- $2p$ and Cl- $2p$ PE spectra. Only a slight sepa-

^{*}stephane.carniato@upmc.fr

ration in the $2p_{3/2}$ line is visible. This is due to the small amount of MF splitting compared to the SO splitting and to the Lorentzian broadening of the core hole states. Indeed the SO splitting is at least ten times greater than the MF splitting in the $2p$ level of sulfur- and chlorine-containing molecules.

In this paper we propose an *ab initio* theoretical description of Si- $2p$ PE spectra of silicon hydride cations $\text{SiH}^+_{(n=1,2,3)}$. This paper is based on the EH model [11,14,19], which is easy to implement and well suited for the interpretation of experimental results. It takes into account SO coupling, electronic relaxation and correlation, and vibrational effects. Contrary to previous works where an empirical value of the γ_{2p} SO coupling parameter was stated, a value was extracted from *ab initio* computations in the SiH_4 molecule, and confirmed by favorable comparison with experimental results [21,22]. Complementary GAMESS (US) [23] implementations of the full Breit-Pauli formalism [24–27] were carried out for tractable numerical executions. Breit-Pauli results served as a benchmark for the validation of our theoretical EH model. Kosugi and Ishida [28] applied successfully an *ab initio* Breit-Pauli approach to the $2p$ ionized states of OCS, SO_2 , and PF_3 .

The purpose of our paper is to study the relative contribution of the SO and MF splittings and to predict their signature on PE spectra. We demonstrate that, in the silicon hydride cations, the absolute values of the SO and MF splittings are of comparable magnitude but their relative signs may differ, leading to substantially different photoelectron spectra. Furthermore, we show that the valence shell occupation in the ground state of these systems controls the sign of the MF splitting. The electronic relaxation and correlation effects on the spectra are also investigated.

The present paper is organized as follows. First, the theoretical approach describing molecular-field, spin-orbit, and vibrational effects is specified. Second, L -edge photoelectron spectra of model systems are discussed in order to obtain detailed insights into the relative SO and MF contributions. Then, the implemented effective Hamiltonian model is checked thanks to the study of the SiH_4 L -edge photoelectron spectrum and its comparison with previous works. Results are presented for the closed-shell systems $\text{SiH}^+_{n=1,3}$. The reasons for the substantially different photoelectron spectra in SiH^+ and in SiH_3^+ are analyzed thoroughly. Results for the more complex open-shell SiH_2^+ system are finally reported.

II. THEORETICAL BACKGROUND

A. Nonrelativistic binding energies

Nonrelativistic properties of ground and core hole states were computed using the GAMESS (US) package [23]. The geometry and the vibrational frequencies of the ground states were optimized at a density-functional theory (DFT) level of theory, with the Becke three-parameter hybrid exchange [29] and the B3LYP Lee-Yang-Parr gradient-corrected correlation functional [30]. Following the results of previous studies [19] large atomic basis sets including f polarization functions were used. A Dunning augmented correlation-consistent polarized core-valence quadruple zeta (aug-cc-pCVQZ) basis set [31] was selected for the silicon and chlorine atomic centers and a Dunning aug-cc-pVQZ basis set [32] was chosen for the

hydrogen centers. Earlier studies discussed which level of theoretical description is necessary in order to provide accurate MF splittings. They concluded that Koopmans's approximation is not suitable [19,20] while a significant improvement is obtained when relaxation of the core hole orbital is taken into account, and reinforced by the inclusion of electronic correlations [13]. Therefore we computed nonrelativistic BEs of the core hole species at a post-Hartree-Fock configuration-interaction (CI) level based on optimized relaxed orbitals, and taking into account single and double excitations (CISD). Relaxed orbitals were optimized for a $2s$ core hole configuration in order to avoid preferential orientation effects. CI(3, n_{val} , n_{vir}) schemes were then developed. The three numbers 3, n_{val} , and n_{vir} indicate, respectively, the number of $2p$ orbitals, of outermost occupied valence orbitals, and of unoccupied orbitals included in the calculation. All these numbers refer to the principal configuration of the ground states. Moreover, occupation restricted multiple active space implementations [33] of CI procedures were driven, in which the occupation number in the $2p$ active space was fixed to $2p^5$. The same active space was used for the ground and core hole states of each species.

In order to analyze the impact on MF splittings of relaxation and correlation effects we also assessed the nonrelativistic BEs of the core hole species at lower levels of theory.

(1) In the case of closed-shell ground-state systems, we applied the frozen core approximation, according to the Koopmans theorem. The nonrelativistic BEs were then obtained as opposite to the Hartree-Fock self-consistent field (SCF) eigenvalues: $E_{x,y}^0 = -\epsilon_{2p_{x,y}}^0$ and $E_z^0 = -\epsilon_{2p_z}^0$.

(2) We implemented restricted CI(3,0,0) schemes in which only the three $2p$ orbitals were included in the active space. This scheme takes only into account relaxation effects and thus mimics a classical Δ SCF procedure where molecular orbitals (MOs) in the core hole final state are fully relaxed at a restricted open-shell Hartree-Fock (ROHF) level of theory.

In all cases and for the sake of simplicity the nonrelativistic BEs were labeled $E_{x,y,z}$ for, respectively, $2p_{x,y,z}^{-1}$ ($2p_{x,y,z}\alpha$) $^{-1}$ or $2\bar{p}_{x,y,z}^{-1}$ ($2p_{x,y,z}\beta$) $^{-1}$ configurations.

B. Effective Hamiltonian model

Following theoretical works developed at the end of the 1990s [10,11,13,14,19], we determined SO binding energies (SO-BEs) of the MF split $2p$ core hole states using the EH model in which the SO interaction is described in the $2p$ level:

$$H_{\text{SO}} = \gamma_{2p} \sum_i \vec{\ell}_i \cdot \vec{s}_i. \quad (1)$$

The earliest theoretical works were designed for cases in which the SO interaction was much larger than the MF splittings. A perturbative description in which MF effects were described inside each J subspace [10] or each M_J subspace [14] could then be applied. But other approaches [11,13,19] dealt with the full Hamiltonian where SO and MF effects were considered simultaneously. Either spectral bases made of $^{2S+1}\Pi_{M_J}$ terms [10,11,14,19] or Cartesian bases made of $^{2S+1}\Pi_{x,y}$ terms [13] were used. The Cartesian bases have the advantage of localizing MF effects in the diagonal elements

and are also well suited for connections with quantum chemistry packages.

Because SO and MF effects are of comparable strengths for the silicon hydrides we applied a nonperturbative procedure taking into account these effects at the same level. We implemented the EH scheme with Cartesian and spectral basis sets. We made the approximation that each $2p$ core hole state was built on a unique configuration, or at least an antisymmetrized combination according to Pauli's principle. Even if the symmetry groups of the molecules studied here are not $C_{\infty v}$ and do not rigorously allow the nomenclature in terms of σ and π orbitals, we characterized nevertheless the Λ quantum numbers in terms of Σ and Π labels in order to have a unique designation for all the molecular species. For example, the Cartesian $|2p_{x,y}^{-1}|$ or $|2\bar{p}_z^{-1}|$ Slater determinants are connected to $\bar{\Pi}_{x,y}$ or Σ labels. Similarly the spectral Λ_{M_J} labels are built from $|2\bar{p}_{m_\ell}^{-1}|$ and $|2p_{m_\ell}^{-1}|$ Slater determinants. The conventions chosen for these determinants are given in Appendices A and B. In the doublet open-shell SiH_2^+ system with one single electron in the valence outermost molecular orbital, this latter orbital is named σ_{HO} .

1. Closed-shell systems

For the closed-shell ground-state molecules SiH^+ and SiH_3^+ , the nonrelativistic BEs of the $2p_x$ and $2p_y$ core hole states are degenerate, so that the differential energy is $\Delta = 0$. In such cases the MF splitting can then be defined as the differential nonrelativistic BE:

$$\Delta_{\text{MF}} = E_z - E_{x/y} \quad (2)$$

where the common $E_x = E_y$ energy is labeled $E_{x/y}$. The Δ_{MF}^0 MF splitting defined according to the Koopmans approximation can be labeled SCF molecular-field splitting. It can also be defined as the MF splitting in the initial state:

$$\Delta_{\text{MF}}^0 = E_z^0 - E_{x/y}^0 = -\epsilon_{2p_z^{-1}}^0 + \epsilon_{2p_{x,y}^{-1}}^0 \quad (3)$$

SO matrices were obtained in Cartesian and in spectral basis sets defined in Appendix A1. The Cartesian matrices (A.28) are identical to those obtained by Fink and coworkers [13]. They correspond to a chosen positive value for the SO parameter. In the spectral bases, each 3×3 H_{SB} matrix displayed in Eq. (A29) is separated in two blocks. The $M_J = \pm \frac{3}{2}$ states are associated to the SO binding energy:

$$E_{\frac{3}{2}} = E_{x/y} - \frac{\gamma_{2p}}{2} \quad (4)$$

In the $|M_J| = 1/2$ subspace the SO Hamiltonian is written

$$H_{\frac{1}{2}} = \begin{pmatrix} {}^2\Pi_{\frac{1}{2}} & {}^2\Sigma_{\frac{1}{2}} \\ E_{x/y} + \frac{\gamma_{2p}}{2} & \frac{\gamma_{2p}}{\sqrt{2}} \\ \frac{\gamma_{2p}}{\sqrt{2}} & E_z \end{pmatrix} \quad (5)$$

The eigenvalues are

$$E_{\pm} = \frac{1}{2} \left[E_{x/y} + E_z + \frac{\gamma_{2p}}{2} \pm \sqrt{\left(\Delta_{\text{MF}} - \frac{\gamma_{2p}}{2} \right)^2 + 2\gamma_{2p}^2} \right] \quad (6)$$

Each of the E_{\pm} levels is associated to a twofold space made of corresponding eigenvectors of the two $H_{\frac{1}{2}}$ matrices.

In the case of the SiH_4 molecule, the three $2p$ core hole nonrelativistic BEs ($E_{2p^{-1}}$) are degenerate, so that $\Delta_{\text{MF}} = 0$ and two SO binding energies are obtained:

$$E_- = E_{\frac{3}{2}} = E_{2p^{-1}} - \frac{\gamma_{2p}}{2} \quad (7)$$

and

$$E_+ = E_{2p^{-1}} + \gamma_{2p} \quad (8)$$

The SO-BEs correspond to the respective atomic cases $2p_{\frac{3}{2}}$ and $2p_{\frac{1}{2}}$.

2. Open-shell systems

For doublet open-shell systems with one single electron in the valence outermost molecular orbital, the MF can completely lift the degeneracy of the three SCF $2p_{x,y,z}$ MO energies. The ionized configurations $2p_x^{-1}\sigma_{\text{HO}}$, $2p_y^{-1}\sigma_{\text{HO}}$, and $2p_z^{-1}\sigma_{\text{HO}}$ lead then to six different nonrelativistic BEs: $E_{3\Pi_x}$, $E_{3\Pi_y}$, $E_{1\Pi_x}$, $E_{1\Pi_y}$, $E_{3\Sigma}$, and $E_{1\Sigma}$. The full 12×12 SO matrix can be split in two 6×6 submatrices using spectral $2S+1 \Lambda_{M_J}$ basis sets satisfying the antisymmetrization postulate and described in Appendix B1. The first 6×6 matrix (denoted H_1) is built in the $|M_J| = 1$ subspace. The second one (denoted H_{02}) is built in the $\{|M_J| = 2, M_J = 0^+, M_J = 0^-\}$ subspace. The two six-dimensional subspaces are obviously not coupled by SO effects according to their different M_J quantum numbers. Nor are they connected by MF effects because the ${}^3\Pi$ (${}^3\Sigma$) states in the two subspaces correspond to $M_S = 0$ ($M_S = \pm 1$) values in one subspace and to $M_S = \pm 1$ ($M_S = 0$) values in the other one. Indeed MF effects can only couple terms with the same S , M_S , and Λ quantum numbers. Thus $M_J = 0$ and $|M_J| = 2$ states are connected in the same 6×6 subspace. In the $M_J = 0$ subspace the basis sets are chosen according to the two irreducible representations $M_J = 0^+$ and $M_J = 0^-$ defined by Herzberg [34].

The 6×6 Hamiltonian H_1 displayed in Eq. (A40) of Appendix B2 can be separated in two 3×3 submatrices according to the two $[{}^1\Pi_-, {}^3\Pi_+, {}^3\Sigma_+]$ and $[{}^1\Pi_+, {}^3\Pi_-, {}^3\Sigma_-]$ subspaces where the new vectors are defined as

$${}^{1,3}\Lambda_{\pm} = \frac{1}{\sqrt{2}} [{}^{1,3}\Lambda_1 \pm {}^{1,3}\Lambda_{-1}] \quad (9)$$

The two subspaces are obviously two irreducible representations of the SO operator. They correspond also to irreducible representations of the nonrelativistic part of the Hamiltonian because the ${}^{1,3}\Pi_{\pm}$ combinations naturally pertain to the Cartesian ${}^{1,3}\Pi_{x,y}^{M_S=0}$ terms:

$${}^{1,3}\Pi_y^0 = i{}^{1,3}\Pi_+ \quad \text{and} \quad {}^{1,3}\Pi_x^0 = -{}^{1,3}\Pi_- \quad (10)$$

The separation occurs then according to the two subspaces: $[{}^1\Pi_y^0, {}^3\Pi_x^0, {}^3\Sigma_-]$ and $[{}^3\Pi_y^0, {}^1\Pi_x^0, {}^3\Sigma_+]$.

The submatrices are, respectively,

$$H_{1a} = \begin{pmatrix} {}^3\Pi_x^0 & {}^1\Pi_y^0 & {}^3\Sigma_- \\ E_{3\Pi_x} & \frac{i\gamma}{2} & -\frac{\gamma}{2} \\ -\frac{i\gamma}{2} & E_{1\Pi_y} & -\frac{i\gamma}{2} \\ -\frac{\gamma}{2} & \frac{i\gamma}{2} & E_{3\Sigma} \end{pmatrix} \quad (11)$$

and

$$H_{1b} = \begin{pmatrix} {}^3\Pi_y^0 & {}^1\Pi_x^0 & {}^3\Sigma_+ \\ E_{3\Pi_y} & -\frac{i\gamma}{2} & -\frac{i\gamma}{2} \\ \frac{i\gamma}{2} & E_{1\Pi_x} & -\frac{\gamma}{2} \\ \frac{i\gamma}{2} & -\frac{\gamma}{2} & E_{3\Sigma} \end{pmatrix}. \quad (12)$$

The second 6×6 Hamiltonian H_{02} is displayed in Eq. (A41) of Appendix B2 and it is already separated in two 3×3 blocks. Both of them contain nondiagonal MF terms. Such nondiagonal terms can be obviously removed if the combinations $\frac{1}{\sqrt{2}}({}^3\Pi_{|2|+} \pm {}^3\Pi_{0+})$ and $\frac{1}{\sqrt{2}}({}^3\Pi_{|2|-} \pm {}^3\Pi_{0-})$ are used. These combinations correspond to the following Cartesian basis sets:

$${}^3\Pi_{x,y}^{\pm} = \frac{1}{\sqrt{2}}({}^3\Pi_{x,y}^{+1} \pm {}^3\Pi_{x,y}^{-1}). \quad (13)$$

The following 3×3 submatrices are finally obtained:

$$H_{02c} = \begin{pmatrix} {}^3\Pi_x^+ & {}^3\Pi_y^- & {}^1\Sigma_0 \\ E_{3\Pi_x} & \frac{i\gamma}{2} & \frac{\gamma}{2} \\ -\frac{i\gamma}{2} & E_{3\Pi_y} & -\frac{i\gamma}{2} \\ \frac{\gamma}{2} & \frac{i\gamma}{2} & E_{1\Sigma} \end{pmatrix} \quad (14)$$

and

$$H_{02d} = \begin{pmatrix} {}^3\Pi_x^- & {}^3\Pi_y^+ & {}^3\Sigma_0 \\ E_{3\Pi_x} & -\frac{i\gamma}{2} & \frac{\gamma}{2} \\ \frac{i\gamma}{2} & E_{3\Pi_y} & -\frac{i\gamma}{2} \\ \frac{\gamma}{2} & \frac{i\gamma}{2} & E_{3\Sigma} \end{pmatrix}. \quad (15)$$

The separation in four submatrices justified here by the existence of quantum invariants is confirmed by the numerical results presented below in Table IV where the eigenvectors are built in three-dimensional subspaces of the appropriate symmetries. These numerical results had been obtained before the separation in four blocks had been operated, by diagonalizing the whole 12×12 Hamiltonian.

C. Vibrational effects

In order to account for eventual vibrational broadenings of the photoelectron spectra, Franck-Condon (FC) factors were evaluated in the harmonic approximation. The geometries and the vibrational frequencies of the Si- $2p$ core excited states in $\text{SiH}^+_{(n=2,4)}$ compounds were optimized at a DFT level of theory with the B3LYP correlation-exchange functional. The inner-shell vacancy was assumed to be located in the $2s$ orbital.

In this approach the normal modes for each excited states are supposed to be the same as those of the ground electronic state. The FC factors for the transition between the fundamental vibrational state of the ground electronic state and the \mathbf{v}_j

vibrational state of the j th electronic state can then be written

$$FC_j(0; \mathbf{v}_j) = \prod_{i=1}^M |(v_j^i | v_0^0)|^2 = \prod_{i=1}^M \frac{a_i^{n_j^i}}{n_j^i!} \exp(-a_i) \quad (16)$$

where M is the number of normal modes v_j^i occupied in the \mathbf{v}_j vibrational state and n_j^i are the quantum numbers for each of these normal modes. The Huang-Rys parameters a_i are defined as

$$a_i = \frac{\Delta q_i^2 \mu_i \omega_i}{2\hbar} \quad (17)$$

where ω_i and μ_i are, respectively, the frequency and the reduced mass of the i th vibrational normal mode. The variations of the normal coordinates Δq_i can be related to those of the Cartesian coordinates thanks to the (A_{ij}) matrix elements for the coordinate transformation. According to the normalization chosen in the GAMES (US) package, Δq_i are defined as follows:

$$\Delta q_i = \sum_{j=1}^{3N} \frac{m_j}{\sqrt{\mu_i}} A_{ij} \Delta X_j. \quad (18)$$

The cross section associated to the photoionization in the \mathbf{v}_j vibrational channel induced by the absorption of a photon of energy ω and producing a photoelectron of energy E is proportional to

$$\sigma_{\mathbf{v}_j}(E) \propto \frac{FC_j(0; \mathbf{v}_j)}{[\omega - (E + I_j + \epsilon_{\mathbf{v}_j} - \epsilon_0^0)]^2 + \frac{\Gamma_j^2}{4}} \quad (19)$$

where $\epsilon_{\mathbf{v}_j}$ and ϵ_0^0 are the vibrational energies associated, respectively, to the excited and ground electronic states, where I_j are the ionization potentials for the adiabatic electronic transitions and Γ_j is the lifetime of the core ionized state j of interest.

The same common lifetime of 95 meV [12] was taken into account for all the Si- $2p$ inner-shell species considered in this paper.

III. RESULTS AND DISCUSSIONS

A. Model study of the imprint on L -edge photoelectron spectra of MF and SO relative strengths

We analyze here how the relative sign and strength of the MF and SO splittings impact the L -edge photoelectron spectra in conceptual cases. We consider models for a closed-shell system with a positive SO parameter and examine positive and negative values of the MF splittings, $|\Delta_{\text{MF}}|$ ranging from $\gamma_{2p}/10$ to $5 \times \gamma_{2p}$. Resulting L -edge photoelectron spectra are displayed in Fig. 1. When $|\Delta_{\text{MF}}|$ is much smaller than γ_{2p} (i.e., $|\Delta_{\text{MF}}| = \gamma_{2p}/10$), only two structures corresponding roughly to $2p_{3/2}$ and $2p_{1/2}$ atomic lines are observable. The 3,2 versus 1,2 ordering is an inverse ordering, which is generally the case in these L -core hole situations [19]. When $|\Delta_{\text{MF}}|$ increases, three peaks can be clearly identified. The energy state ordering is $E_- < E_{3/2} < E_+$ when $\Delta_{\text{MF}} < 0$ and $E_{3/2} < E_- < E_+$ when $\Delta_{\text{MF}} > 0$. When $|\Delta_{\text{MF}}|$ reaches half of the SO parameter, two close peaks and a third one well differentiated appear (the noted 2 + 1 scheme in the following). The two close ones correspond to the separation by the

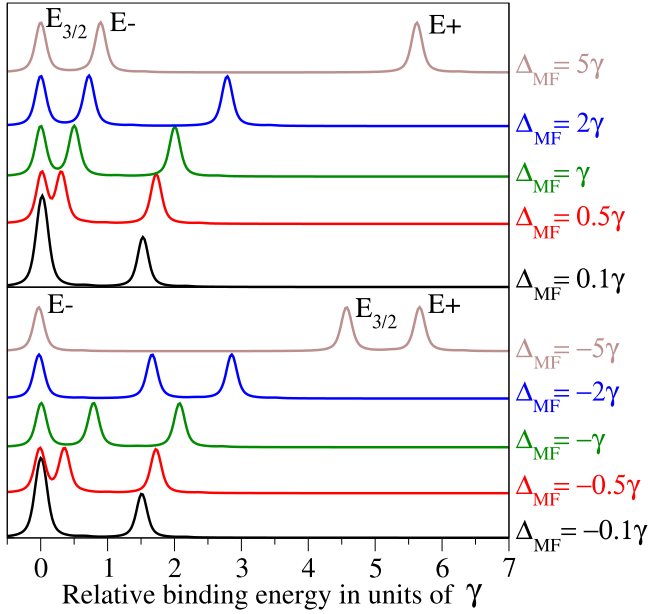


FIG. 1. Evolution of L -edge theoretical photoelectron spectra with the relative strength of MF and SO splittings. Top panel: $\Delta_{\text{MF}} > 0$ case. Bottom panel: $\Delta_{\text{MF}} < 0$ case. The lowest-energy lying peak of each simulation is chosen as the origin of the energy scale.

molecular field of the quasiatomic $2p_{3/2}$ line. The study of these two cases (black and red curves) reveals thus that the spectra corresponding to $\Delta_{\text{MF}} < 0$ and $\Delta_{\text{MF}} > 0$ cannot be differentiated at first sight when $|\Delta_{\text{MF}}|$ is significantly smaller than the SO parameter. A complementary spectroscopic analysis could reveal, however, the different molecular symmetry orderings: ${}^2\Pi_{3/2}$, ${}^2\Pi_{1/2}$, and ${}^2\Sigma_{1/2}$ in the $\Delta_{\text{MF}} > 0$ case and ${}^2\Sigma_{1/2}$, ${}^2\Pi_{3/2}$, and ${}^2\Pi_{1/2}$ in the $\Delta_{\text{MF}} < 0$ case. Determining these orderings would provide the sign of the MF splitting. Such a complementary spectroscopic tool could be the Auger spectroscopy.

When the absolute value of the MF splitting becomes slightly larger than the SO effects (i.e., $|\Delta_{\text{MF}}| = 2 \times \gamma_{2p}$), the sign of the MF splitting influences substantially the shape of the spectrum: for positive MF splittings the distance between the third and the second peaks is always greater than that between the second and the first peaks. In contrast, for negative MF splittings the energy difference between the second and the third peaks becomes smaller than that between the first and the second peaks (i.e., the 1 + 2 scheme). In both cases, the relative distances between the peaks become similar (the 1 + 1 + 1 scheme) when $|\Delta_{\text{MF}}| = \frac{3}{2}\gamma$ (not shown). In the limit where $|\Delta_{\text{MF}}| \gg \gamma$ the main separation Π/Σ is generated by the MF effects while the SO splitting breaks slightly the degeneracy between the two ${}^2\Pi_{3/2}$ and ${}^2\Pi_{1/2}$ components. This induces a 1 + 2 scheme in the $\Delta_{\text{MF}} < 0$ case where the E_+ peak corresponds to the ${}^2\Pi_{1/2}$ term and a 2 + 1 scheme in the $\Delta_{\text{MF}} > 0$ case where the E_- peak corresponds to the ${}^2\Pi_{1/2}$. Such schemes would make it possible to characterize at first sight the sign of MF splittings.

In our paper, we consider silicon hydride cations in which SO and MF splittings are of comparable magnitude ($|\Delta_{\text{MF}}| \approx \gamma_{2p}$). As shown in Fig. 1, in this case the L -edge photoelectron spectrum can provide straightforward information on the sign

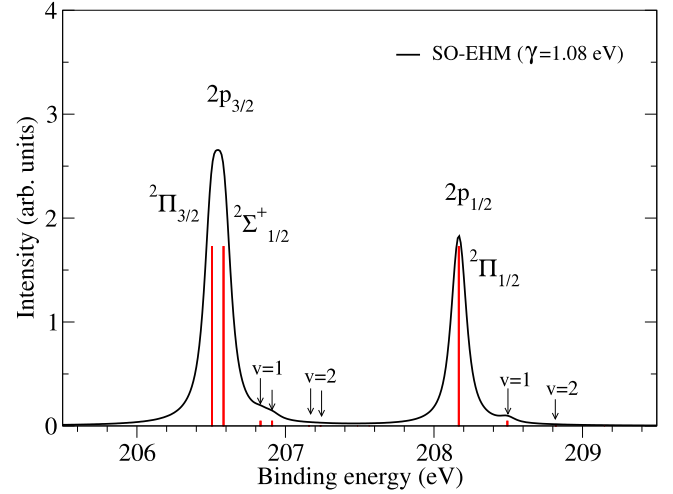


FIG. 2. L -edge photoelectron spectrum of HCl computed at the CISD (3,4,143) level.

of the MF splitting: for a positive Δ_{MF} the spectrum exhibits a 2 + 1 scheme while for a negative Δ_{MF} a 1 + 1 + 1 scheme is observed.

B. L -edge photoelectron spectrum of HCl: Weak imprint of MF splittings

We analyze in this paragraph the L -edge photoelectron spectrum of hydrogen chlorine, which has been already widely investigated and which is the typical example for standard molecular L -edge photoelectron spectra. Hydrogen chlorine belongs to the $C_{\infty v}$ group of symmetry. Its fundamental term is ${}^1\Sigma^+$ and the electronic configuration is $1\sigma^2 2\sigma^2 3\sigma^2 1\pi^4 4\sigma^2 5\sigma^2 2\pi^4$. The 1σ , 2σ , 3σ , and 1π orbitals are essentially the $1s$, $2s$, $2p_z$, and $2p_{x,y}$ chlorine atomic orbitals, respectively. The 1π MOs correspond to degenerate energies. The $2p_\sigma$ orbitals being more stable compared to the $2p_{\pi_{x,y}}$ ones, the SCF molecular-field splitting is positive. The Koopmans theorem computed value is 40 meV. The MF splitting remains positive when considering higher levels of theory. For example, we obtain 123 meV in a CISD (3,4,143) scheme. This latter value is in very good agreement with previous theoretical CI evaluations [13,20].

The first photoelectron spectrum in which MF splitting of $2p$ core hole states was resolved in HCl was recorded by Aksela and coworkers [12]. This experimental study revealed a SO parameter of $\gamma_{2p} = 1.08$ eV. In that case the SO effect is thus around ten times larger than the MF effects. Indeed, according to the black curves in Fig. 1 the photoelectron spectrum displayed an atomic shape with two bands corresponding mainly to the $2p_{3/2}$ and $2p_{1/2}$ lines. The photoelectron spectrum we modeled is displayed in Fig. 2. It was obtained using nonrelativistic BEs modeled in a CISD (3,4,143) scheme. The theoretical intensities were convoluted by a Gaussian function of 50-meV full width at half maximum that reproduces the experimental resolution. This same operation was carried on for all the simulated spectra presented in this paper. Note that recent works on Cl- $2p$ photoelectron spectra evidenced the role played by molecular-field effects on the lifetime broadening of the core ionized states [15]. However, such effects are smaller

than those of the relative MF and SO effects and are thus not considered in our paper. As expected, the photoelectron spectrum exhibits mainly two intense bands and some shoulders on the high-energy side of each of these bands. These shoulders are the signature of weak vibrational progressions. These latter are due to a slight increase of the bond length (+2 pm) in the core ionized species. Apart from these weak progressions, the photoelectron spectrum appears essentially as an atomic spectrum: the two main bands are separated by $3.2 \gamma_{2p} \sim 1.62$ eV and the relative ratio of the peak surfaces is about the atomic multiplicity value of 2. The ${}^2\Pi_{3/2}$ and ${}^2\Sigma_{1/2}$ molecular components are 76 meV apart. In the experimental spectrum by Aksela and coworkers [12], a decomposition of the $2p_{3/2}$ line in two elements with the same shape and the same width could be carried out and revealed a distance of 79 ± 8 meV between the ${}^2\Pi_{3/2}$ and $\Sigma_{1/2}$ molecular components, in good agreement with our CISD (3,4,143) value.

C. SiH₄: Determination of the SO parameter and validation of the effective Hamiltonian model

We first consider the silane molecule in order to (i) determine the numerical value for the SO coupling parameter γ_{2p} for silicon and (ii) validate the effective Hamiltonian model by comparing the *L*-edge photoelectron spectrum with available experimental data [21,22].

Silane SiH₄ belongs to the T_d group of symmetry. Its fundamental term is 1A_1 and its closed-shell electronic configuration is $1a_1^2 2a_1^2 1t_2^6 3a_1^2 2t_2^6$. The $1a_1$, $2a_1$, and $1t_2$ orbitals are essentially the silicon $1s$, $2s$, and $2p_{x,y,z}$ orbitals. The fully occupied bonding $3a_1$ and $2t_2$ valence MOs are mainly built, respectively, on (Si $3s$ -H $1s$) and (Si $3p$ -H $1s$) combinations. As expected for a molecule of T_d symmetry, the $1t_2$ ($2p_{x,y,z}$) molecular orbitals are energy degenerated. There is thus no MF splitting in this molecule. The DFT/B3LYP SiH interatomic distance and symmetric ν_{SiH} stretching frequency are, respectively, 1.479 Å and 2236 cm^{-1} , in good agreement with experimental data [22] (1.4798 Å and 2187 cm^{-1}). The Si-H equilibrium distance is 1.424 Å and the symmetric stretching frequency is 2470 cm^{-1} in the $2p$ core hole molecule. The stretching frequency thus increases while the Si-H distance decreases significantly when a core hole is produced. This behavior indicates that the electronic relaxation is important in the core hole molecule and strengthens the bond.

The SO parameter was determined by comparing the SO splittings obtained at the CI(3,0,0) level of theory with the EH model and with a relativistic Breit-Pauli calculation. The $\gamma_{2p} = 0.407$ eV value was obtained. With this value the SO splitting between the two atomic $2p_{3/2}$ and $2p_{1/2}$ lines, $\Delta_{\text{SO}} = \frac{3}{2}\gamma_{2p}$, amounts to 0.610 eV, in good agreement with the experimental value of 0.612 eV [22]. The SO binding energies for the fundamental vibrational levels are 106.70 and 107.31 eV for the $2p_{3/2}$ and the $2p_{1/2}$ lines, respectively. This latter value is in good agreement with the experimental one of 107.28 eV [21] or 107.31 ± 0.05 eV [22]. Correlation effects taken into account when implementing a CI(3,4,93) procedure do not improve the agreement.

The *L*-edge photoelectron spectrum for SiH₄, simulated with a lifetime broadening of 45 meV [22], is displayed in Fig. 3. The nuclear vibration along the symmetric stretching

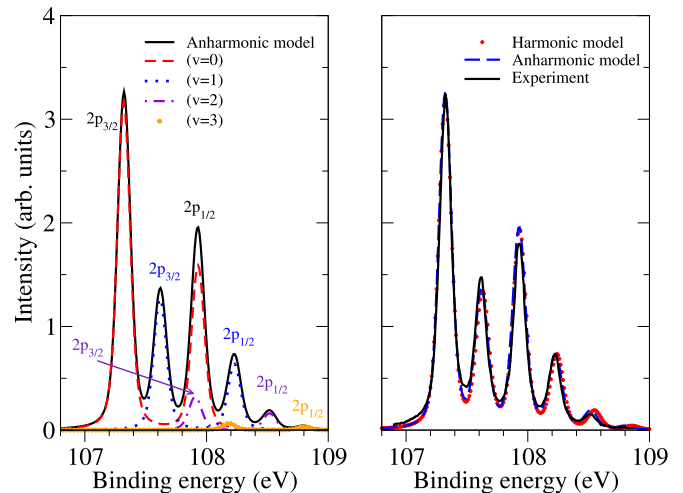


FIG. 3. Si *L*-edge photoelectron spectrum of SiH₄ simulated at the CI (3,0,0) level of theory. Vibrational progression is accounted for up to the third excited state. The anharmonic model is applied in the left panel. In the right panel both harmonic and anharmonic models are displayed, in comparison with experimental results [22]. The Si- $2p$ core hole lifetime width is set to 95 meV.

mode was taken into account up to the third excited vibrational level. A vibrational progression is clearly visible because the Si-H bond length is significantly shortened (≈ -5.5 pm) in the $2p$ core hole state. The spectrum consists of six bands that reproduce quite well the experimental bands clearly identified by Bozek *et al.* [22]. The harmonic vibrational splitting was found close to 0.31 eV in good agreement with the observed experimental splitting (0.295 eV). The Franck-Condon factors of 65.4, 26.3, and 6.67% were obtained for the ground, first excited, and second excited vibrational states ($v = 0, 1, 2$) of the core hole ion, respectively, in very good agreement with the experimental data (66.3, 29.1, and 4.6%). We also show in Fig. 3 the spectrum obtained by taking into account the first anharmonic correction $\Delta_v = -\omega x_e(v + \frac{1}{2})^2$. The anharmonic parameter ωx_e was estimated around 22 cm^{-1} by fitting the experimental results. The theoretical SO energies were rescaled so that the anharmonic $v = 0$, $2p_{3/2}$ value corresponds to the experimental value of 107.31 eV. The anharmonic correction improves only slightly the overall agreement, i.e., only for high-lying ($v \geq 2$) vibrational levels, with the experiment and is thus not considered for the spectra of the silicon hydride cations.

D. *L*-edge photoelectron spectrum of silicon hydride cations: Strong effect of MF splittings

1. SiH⁺ versus SiH₃⁺: SCF ground states

The silyl cation SiH₃⁺ is planar and belongs to the D_{3h} group of symmetry. Its electronic closed-shell configuration is $1a_1^2 2a_1^2 1a_1'^2 1e'^4 3a_1'^2 2e'^4$ and its fundamental term is ${}^1A_1'$. The $1a_1'$, $2a_1'$, $1a_1''$, and $1e'$ orbitals are essentially the silicon $1s$, $2s$, $2p_z$, and $2p_{x,y}$ orbitals. The degenerated highest occupied molecular orbitals (HOMOs) of symmetry e' display a large bonding character built mainly on a combination of two of the three atomic H ($1s$) orbitals and an antibonding character built mainly on a combination between the Si $3p_{x/y}$

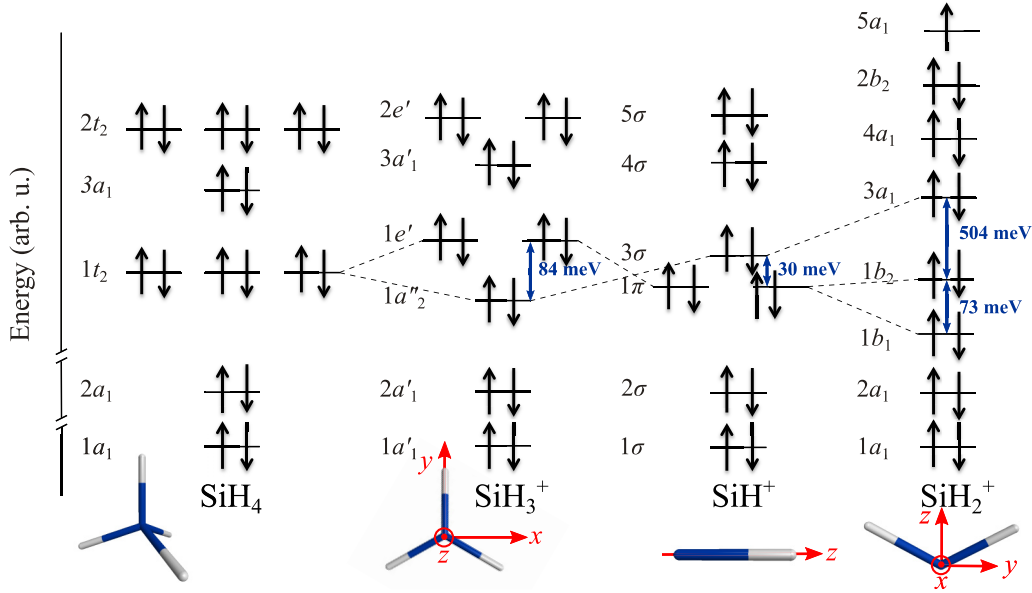


FIG. 4. SCF molecular orbital ordering of the silicon species. The z axis is chosen along the principal axis.

and the third H ($1s$) atomic orbitals. The lowest unoccupied MO (LUMO) $2a'_2$ is perpendicular to the molecular plane and corresponds mainly to the $3p_z$ silicon atomic orbital.

The silicon monohydride cation SiH^+ belongs to the $C_{\infty v}$ group of symmetry. Its fundamental term is $^1\Sigma^+$ and its closed-shell electronic configuration is $1\sigma^2 2\sigma^2 1\pi^4 3\sigma^2 4\sigma^2 5\sigma^2$. The 1σ , 2σ , 1π , and 3σ orbitals are essentially the silicon $1s$, $2s$, $2p_{x,y}$, and $2p_z$ orbitals. The HOMO and (HOMO-1) (penultimate occupied MO) are of symmetry σ and correspond, respectively, to antibonding and bonding combinations of H- $1s$ and Si $3s$ - $3p_z$ hybrid orbitals. The two 2π LUMOs correspond mainly to the $3p_x$ and $3p_y$ silicon atomic orbitals.

A schematic diagram displaying the SCF molecular orbital energy ordering is given in Fig. 4. This ordering is the reverse image of the SCF molecular-field splitting defined in Eq. (2). In SiH_3^+ the $2p\sigma$ ($1a'_2$) MO is more stable than the $2p_{\pi_{x,y}}$ ($1e'$) MOs, so that the SCF molecular-field splitting is positive for this cation. The result is just the contrary in the SiH^+ case.

2. SiH^+ versus SiH_3^+ : Nonrelativistic BEs of the $2p$ core hole states

Nonrelativistic BEs of core hole states in SiH^+ and SiH_3^+ molecules are summarized in Table I according to four

schemes. The comparison between the Koopmans and CI (3,0,0) results gives an evaluation of the core hole relaxation effects. The comparison between CI (3,0,0) and the minimal CISD results provides an estimate of the electronic correlation effects inside the $(3s, 3p)$ valence shell. The comparison between the two CISD results allows us to assess the electronic correlation effects of the outermost unoccupied orbitals.

There is an overall negative shift of the SiH_3^+ $2p$ core hole binding energies with respect to the SiH^+ ones varying from ≈ -1 to ≈ -2 eV. This shift is partly due to larger screening effects in the initial state and partly due to larger relaxation effects in the core hole species, both coming from the presence of two extra hydrogen atoms. The MF splittings Δ_{MF} are displayed in the last line of Table I. They are of opposite sign in the two molecules and in both cases their sign is preserved regardless of the implemented level of theory. An important conclusion can then be drawn: the sign of the MF splitting in the $2p$ core hole states shows as a mirror the SCF molecular orbital ordering of the silicon species. Therefore we can discuss the MF splittings, without having to specify if we refer to initial or core hole states. Another characteristic of the MF splittings concerns their evolution with the level of theory. Their absolute value increases when going from the Koopmans to the largest CISD scheme. The evolution of the MF splitting is more significant when going from the

TABLE I. Nonrelativistic binding energies (in eV) of $2p$ core hole states in SiH^+ and in SiH_3^+ computed at the Koopmans, ΔSCF (CI (3,0,0)), and two CISD ($3, n_{\text{val}}, n_{\text{vir}}$) levels. The MF splittings are displayed in the last row. See text for more details.

	SiH^+			SiH_3^+				
	Koopmans	ΔSCF	CISD	Koopmans	ΔSCF	CISD		
		3,0,0	3,2,2	3,2,145		3,0,0	3,3,1	3,3,144
$2p_{\sigma-1}$	125.12	118.55	118.064	117.88	124.31	117.05	116.978	116.72
$2p_{\pi-1}$	125.15	118.65	118.448	118.32	124.22	116.90	116.747	116.43
Δ_{MF}	-0.03	-0.10	-0.384	-0.44	+0.09	+0.16	+0.231	+0.29

TABLE II. Spectral terms, binding energies (in eV), and compositions of the $2p$ core hole SO eigenstates computed at the Koopmans, CI (3,0,0), and CISD (3,2,145) levels for SiH^+ and at CI (3,0,0) and CISD (3,3,144) levels for SiH_3^+ . The distance between the SO states split by the molecular field, $\Delta_{\text{MF}}\text{SO} = E_- - E_{3/2}$, is given in the last row. See text for more details.

	SO-Koopmans				SO-CI(3,0,0)				SO-CISD(3,2,145)				${}^2\Lambda_{M_J}$
	Energy	Composition			Energy	Composition			Energy	Composition			
SiH^+		$2p_x^{-1}$	$2p_y^{-1}$	$2p_z^{-1}$		$2p_x^{-1}$	$2p_y^{-1}$	$2p_z^{-1}$		$2p_x^{-1}$	$2p_y^{-1}$	$2p_z^{-1}$	
E_-	124.92	15.6	15.6	68.8	119.07	13.3	13.3	73.3	117.77	6.12	6.12	87.5	${}^2\Sigma_{1/2}$
$E_{3/2}$	124.94	50.0	50.0	0.0	119.14	50.0	50.0	0.0	118.12	50.0	50.0	0.0	${}^2\Pi_{3/2}$
E_+	125.54	34.4	34.4	31.2	119.72	36.6	36.6	26.7	118.64	43.7	43.7	12.5	${}^2\Pi_{1/2}$
$\Delta_{\text{MF}}\text{SO}$	-0.02				-0.07				-0.350				
	SO-CI(3,0,0)				SO-CISD(3,3,144)								
SiH_3^+	Energy	Composition			Energy	Composition							${}^2\Lambda_{M_J}$
$E_{3/2}$	116.694	50.0	50.0	0.0	116.226	50.0	50.0	0.0					${}^2\Pi_{3/2}$
E_-	116.786	22.7	22.7	54.6	116.384	28.5	28.5	42.9					${}^2\Pi_{1/2}$
E_+	117.364	27.3	27.3	45.4	116.966	21.9	21.9	57.1					${}^2\Sigma_{1/2}$
$\Delta_{\text{MF}}\text{SO}$	0.092				0.158								

Koopmans approximation to the ΔSCF description in SiH^+ than in SiH_3^+ . Comparison of ΔSCF and intrashell CI values indicates that intrashell correlation effects are responsible for a large amount of the correlation in both cases: they represent 87% (0.384,0.44) and 79% (0.231,0.29) of the Δ_{MF} values for, respectively, SiH^+ and SiH_3^+ . We evaluate also the impact of intrashell valence correlation effects on absolute nonrelativistic $2p_\sigma$ and $2p_\pi$ core hole state energies. These absolute energies are lowered for the SiH^+ molecule by, respectively, 0.89 and 0.605 eV in the CI(3,2,2) scheme compared to the ΔSCF values. These variations, compared to those obtained for the CISD(3,2,145) scheme, indicate then that intravalence shell excitations represent a significant amount of approximately 30% of the full CISD(3,2,145) correlation energy in the SiH^+ case. In contrast, in the SiH_3^+ case, intrashell correlation energy was estimated to a small amount (around 5%) of the full CISD (3,3,144) correlation energy.

3. SiH^+ versus SiH_3^+ : SO binding energies and L-shell photoelectron spectra

SO binding energies and compositions of the $2p$ core hole SO eigenstates obtained in the effective Hamiltonian model at different levels of theory are summarized in Table II. Due to an opposite sign for the MF splitting, the ordering between the E_- and $E_{3/2}$ states is reversed in SiH_3^+ compared to that in SiH^+ (see Sec. III A). The SO eigenstates are labeled by the molecular spectral term of the main configuration taking place in the largest CISD scheme. These labels appear in the last column of Table II. Of course these spectral labels are only indicative labels as SO states appear as mixings of different molecular symmetries.

In the SiH^+ case a Σ or Π character is dominant for each Koopmans state and these characters are even reinforced in the CI results. In the Koopmans description the relative amounts of the E_- state approach 1,6, 1,6, and 2,3, which would be the ratios obtained for an atomic $|M_J| = 1,2, 2p_{3/2}$ state. Similarly, the relative ratios of the E_+ state approach 1,3,

1,3, and 1,3, which would be the ratios obtained for each atomic $2p_{1/2}$ state. Indeed, in the Koopmans case the Δ_{MF}^0 MF splitting is small compared to the SO splitting, so that the situation is a quasiatomic one. In the large CISD description, which corresponds to the strongest MF effects, the Σ and Π characters are largely dominant for the SiH^+ case. The states of energy E_- are largely built (87.5%) on $2p_z$ core hole configurations while the states of energy E_+ are largely built (87.5%) on $2p_{x,y}$ core hole ones. They are so labeled, respectively, thanks to the ${}^2\Sigma_{1/2}$ and ${}^2\Pi_{1/2}$ terms. The ${}^2\Pi_{3/2}$ levels are easily identifiable; they are purely made of $2p_\pi$ core hole components. In the SiH_3^+ case, the Σ and Π characters are less pronounced. The proportions of the Σ and Π contributions are even reversed when going from the ΔSCF to the CISD results. For both molecules the energy separation of the two E_- and $E_{3/2}$ peaks increases when CISD calculations including the whole set of valence orbitals and taking into account electronic correlation effects are employed.

The theoretical photoelectron spectra of SiH^+ and SiH_3^+ were simulated under the same conditions as those detailed for SiH_4 . The spectra are displayed in Fig. 5. In SiH^+ core hole ionization produces a very small shortening of the Si-H bond, so that no clear vibrational progression is observed in the L-shell spectra. In SiH_3^+ no vibrational excitation is observable because there is nearly no change of the Si-H length in the $2p$ ionization process. Information on molecular characteristics of the initial and final states of the silicon hydrides is given in Appendix C.

The SiH_3^+ spectrum exhibits a 2 + 1 structure: the ordering is ${}^2\Pi_{3/2}$, ${}^2\Pi_{1/2}$, and ${}^2\Sigma_{1/2}$, as if the 2 + 1 structure is a degeneracy breakdown operated by the SO effect among the Π component of the MF structure. The SiH^+ spectrum is different from the SiH_3^+ one. Indeed, in the SiH^+ case MF and SO strengths are comparable, at least at the CISD (3,2,145) level, but more importantly the MF splitting is of opposite sign as that in SiH_3^+ . The ordering is now ${}^2\Sigma_{1/2}$, ${}^2\Pi_{3/2}$, and ${}^2\Pi_{1/2}$. In that case the structure is rather characterized as a 1 + 1 + 1 structure. Therefore, the $E_- - E_{3/2}$ difference cannot be used

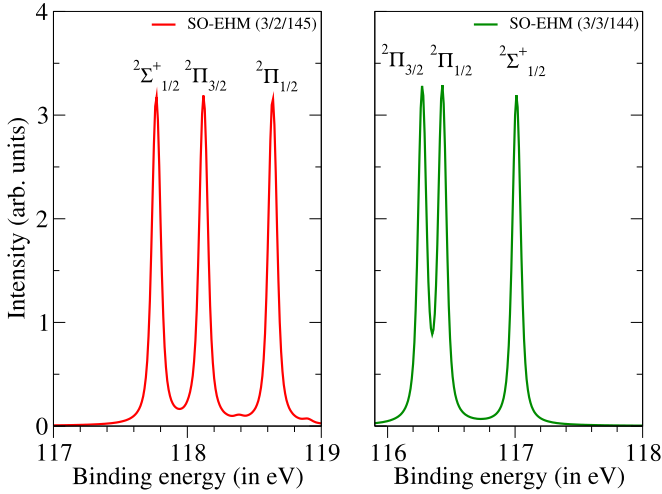


FIG. 5. L -edge photoelectron spectra of SiH^+ (left panel) and SiH_3^+ (right panel) computed at, respectively, the CISD-(3,2,145) and CISD-(3,3,144) level. The Si- $2p$ core hole lifetime width is set to 95 meV.

to define the distance between the SO states split by the molecular field.

SiH^+ and SiH_3^+ molecules are thus two suitable candidates to experimentally investigate the imprint on the L -edge photoelectron spectra of the MF and SO relative strength and sign as discussed in Sec. III A for model systems.

4. Impact of valence shell occupation on the sign of MF splittings

In order to extend our understanding about the impact of molecular effects on the L -edge photoelectron spectra we go further into the analysis of the signs of the MF splittings in the core hole states. Thus we study the energy ordering of the SCF molecular orbitals, as this ordering was demonstrated in Sec. III C 3 to reveal as a mirror these signs.

The opposite energy ordering of the $2p\sigma$ and $2p\pi_{x,y}$ SCF molecular orbitals in SiH^+ compared to that in SiH_3^+ can be partly explained by a different occupation of the outermost molecular orbitals in the two molecules. In SiH_3^+ , the fully occupied HOMOs $2e'$ are mainly built on Si $3p_{x,y}$ orbitals, while the ($2a''_2$) MO, mainly built on the $3p_z$ Si atomic orbital, is unoccupied. In SiH^+ the MO mainly built on the $3p_z$ Si atomic orbital is the fully occupied (5σ) HOMO, as the (2π) MO mainly built on the Si $3p_{x,y}$ orbitals is unoccupied. Penetration of $3p_z$ electrons shields preferentially the nuclear charge seen by the $2p_z$ electrons, while penetration of $3p_{x,y}$ electrons shields preferentially the nuclear charge seen by the $2p_{x,y}$ electrons. This effect is similar to the orientation effect stated by Svensson's rule. Thus the $1e'$ (mainly $2p_{x,y}$) electrons experiment with a smaller nucleus charge and the $1e'$ SCF orbital energy is increased in SiH_3^+ , while the 3σ (mainly $2p_z$) electrons experiment with a smaller nucleus charge and the 3σ SCF orbital energy is increased in SiH^+ .

To reinforce these observations restricted Hartree-Fock calculations performed on a modeled Si atom with the valence closed-shell $1s^2 2s^2 2p^6 3s^2 3p_z^2 3p_{x,y}^0$ configuration show that the $2p_{x,y}$ orbitals are more stable (by an amount of ≈ 50 meV) than the $2p_z$ one.

To further support this interpretation, we investigated the paradigm HCl^{4+} molecule, which is isoelectronic with the SiH^+ molecule, and compared it with HCl presented above. The simulations for HCl^{4+} were performed at the equilibrium nuclear distance of the neutral HCl molecule and the SO effect was described with the SO parameter derived in the HCl molecule: $\gamma_{2p} = 1.08$ eV [14,15]. The two outermost occupied MOs ($4\sigma^2 5\sigma^2$) in HCl^{4+} are built from ($3s-3p_z$) hybrid atomic orbitals, similarly to what happens in the SiH^+ molecule. We obtained for the $2p$ core hole HCl^{4+} molecule MF splitting values of $\Delta_{\text{MF}} = -70, -195, \text{ and } -1289$ meV at the Koopmans, CI (3,0,0), and CISD (3,2,145) level of theory, respectively. All of these splittings are two or three times larger compared to those in the SiH^+ $2p$ core hole, but of the same sign. The CISD values are increased by a factor of 20 compared to the Koopmans values, but it is a comparable factor of 15 in the SiH^+ case. Moreover the ratio between the MF splittings and the SO parameter is the same in the two HCl^{4+} and SiH^+ core hole molecules, so that the HCl^{4+} -HCl couple mimics the SiH^+ - SiH_3^+ one. But the most significant difference between HCl^{4+} and HCl is the presence in HCl of four extra electrons in the outermost 2π orbitals. These orbitals are built on the $3p_{x,y}$ Cl atomic orbitals. Due to the screening effects detailed above, the SCF energy of the 1π orbitals is increased in HCl. The four supplementary 2π electrons in HCl and their selective screening effects thus inverse the ($2p\sigma, 2p\pi_{x,y}$) ordering compared to that taking place in HCl^{4+} . The MF splittings are of opposite sign in the HCl^{4+} and HCl molecules.

E. SiH_2^+

We now investigate the L -edge photoelectron spectrum of the SiH_2^+ molecule. The latter being an open-shell system, the corresponding spectrum is quite complicated. The above discussion on SiH_3^+ and SiH^+ cases helps, however, its interpretation.

The triatomic SiH_2^+ cation belongs to the C_{2v} group of symmetry. Its electronic open-shell configuration is $1a_1^2 2a_1^2 1b_1^2 1b_2^2 3a_1^2 4a_1^2 2b_2^2 5a_1$. Its fundamental term is 2A_1 . The $1a_1, 2a_1, 1b_1, 1b_2,$ and $3a_1$ orbitals are essentially the silicon $1s, 2s, 2p_x, 2p_y,$ and $2p_z$ orbitals. The HOMO $5a_1$ is mainly built on the $3p_z$ silicon atomic orbital. The (HOMO-1) $2b_2$ is mainly localized on the two hydrogen atoms and displays an antibonding character with the $3p_y$ silicon atomic orbital. The LUMO $2b_1$ is perpendicular to the molecular plane and corresponds mainly to the $3p_x$ silicon atomic orbital. As discussed in the previous section, the SCF molecular orbital energy ordering, displayed in Fig. 4, can be connected to the valence shell occupation and its induced screening effects. Indeed, the binding to the nucleus of the $1b_2$ electrons is weakened by the screening effect of the outer $2b_2$ electrons and that of the $3a_1$ electrons is even more weakened by the more numerous outer electrons of symmetry a_1 .

The nonrelativistic energies of the six different $^1,^3\Pi_{x,y}$ and $^1,^3\Sigma 2p^{-1}$ states of the SiH_2^+ molecule are summarized in Table III for a CISD (3,2,95) scheme. The SO energies and the compositions of the corresponding eigenstates are collected in Table IV. The labels (a)–(d) refer to the 3×3 submatrices described in Eqs. (10), (11), (13), and (14). The

TABLE III. Spectral terms and CISD (3,2,95) nonrelativistic binding energies (in eV) of the $2p$ core hole states in SiH_2^+ .

Term	$^3\Sigma$	$^3\Pi_y$	$^3\Pi_x$	$^1\Pi_y$	$^1\Pi_x$	$^1\Sigma$
BE	116.76	117.02	117.27	117.28	117.61	118.05

spectroscopic signatures of the 12 relativistic subcomponents are also reported in Table IV.

The simulated photoelectron spectra are displayed in Fig. 6 for different CI schemes. The ΔSCF spectrum implemented in the CI (3,0,0) scheme is plotted in the left panel.

Since SiH_2^+ is an open-shell system and thus differs significantly from the benchmark silane molecule, we have computed its Breit-Pauli spectrum in order to check the effective Hamiltonian model. Even if it is not reported in the left panel, it coincides within the thickness of the line with the effective Hamiltonian model spectrum. Such a favorable comparison validates the value of the SO parameter ($\gamma_{2p} = 0.407$ eV) and the effective Hamiltonian model for the SiH_2^+ molecule.

The right panel of Fig. 6 displays the spectrum resulting from the largest CISD (3,2,95) calculations. In each panel six bands and 12 components are visible. The 12 components appear in the same order in both CI schemes. The evolution between the two spectra is tenuous. The main difference consists in a shift of the highest-energy lying peak (XII). Different arrangements of peaks IX and X are also observable. The first band is composed by three (I, II, III) quasidegenerate states mainly built from triplet $2p_z^{-1}5a_1^1$ configurations. They are the eigenstates of matrices (d), (b), and (a) essentially built on the $^3\Sigma^0$, $^3\Sigma_+$, and $^3\Sigma_-$ nonrelativistic components, respectively. The second band contains four components. The first three ones (IV, V, VI) are states mainly built from triplet

TABLE IV. SO binding energies (in eV) and compositions of the $^{3,1}(2p^{-1}5a_1^1)$ triplet and singlet states of the SiH_2^+ molecule computed at the CISD (3,2,95) level. The labels (a)–(d) refer to the different matrices described in Eqs. (10), (11), (13), and (14). The spectroscopic terms are defined in Appendix B and in Eqs. (9) and (12).

Term	Energy	Composition					
		Triplet			Singlet		
		$2p_y^{-1}$	$2p_x^{-1}$	$2p_z^{-1}$	$2p_y^{-1}$	$2p_x^{-1}$	$2p_z^{-1}$
I (d) $^3\Sigma_0$	116.590	15.0	2.8	82.3	0.0	0.0	0.0
II (b) $^3\Sigma_+$	116.595	18.0	0.0	81.0	0	1.0	0
III (a) $^3\Sigma_-$	116.612	0.0	5.7	89.0	5.4	0.0	0.0
IV (c) $^3\Pi_y^-$	116.857	78.8	20.6	0.0	0.0	0.0	0.6
V (d) $^3\Pi_y^+$	116.88	59.8	35.3	4.8	0.0	0.0	0.0
VI (b) $^3\Pi_y^0$	116.965	71.0	0.0	12.4	0.0	16.6	0.0
VII (a) $^3\Pi_x^0/{}^1\Pi_y^0$	117.02	0.0	50.7	0.0	49.3	0.0	0.0
VIII (c) $^3\Pi_x^+$	117.237	16.5	72.4	0.0	0.0	0.0	11.2
IX (d) $^3\Pi_x^-$	117.443	25.2	61.8	12.9	0.0	0.0	0.0
X (a) $^3\Pi_x^0/{}^1\Pi_y^0$	117.530	0.0	43.6	11.1	45.3	0.0	0.0
XI (b) $^1\Pi_x^0$	117.693	11.0	0.0	6.6	0.0	82.4	0.0
XII (c) $^1\Sigma$	118.108	4.7	7.0	0.0	0.0	0.0	88.3

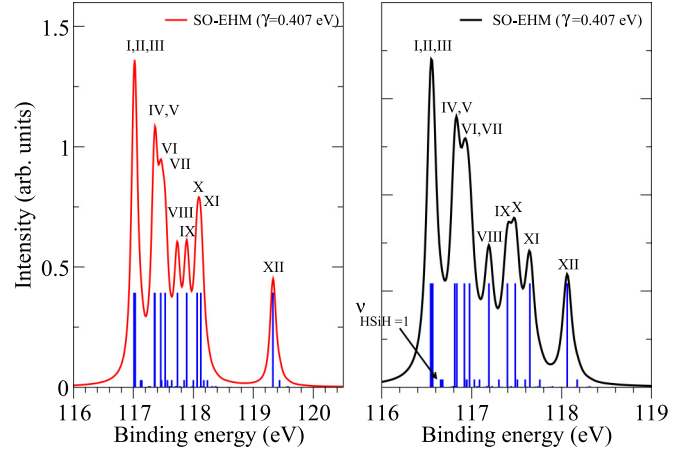


FIG. 6. L -edge SiH_2^+ theoretical photoelectron spectra for different CI schemes. Left panel: ΔSCF results for the CI (3,0,0) scheme. Right panel: Largest CISD (3,2,95) scheme. The Si- $2p$ core hole lifetime width is set to 95 meV.

$2p_y^{-1}5a_1$ configurations. They are eigenstates of matrices (c), (d), and (b) essentially built, respectively, from $^3\Pi_y^-$, $^3\Pi_y^+$, and $^3\Pi_y^0$ nonrelativistic states. Peaks VII and X are eigenstates of matrix (a). They are equivalent mixtures of $^3\Pi_x^0$ and $^1\Pi_y^0$ contributions. Bands VIII and IX correspond to eigenstates of, respectively, matrix (c) and (d) mainly built from $2p_x^{-1}5a_1^1$ configurations. Band XI is the eigenstate of matrix (b) corresponding essentially to the singlet $2p_x^{-1}5a_1^1$ configuration. Band XII is the eigenstate of matrix (c) corresponding essentially to the $^1\Sigma$ term.

Obviously the open-shell spectrum is more complex than the previous closed-shell spectra. The $2p^{-1}5a_1^1$ open-shell ionized configuration is similar to a configuration that could be reached after the $2p \rightarrow 5a_1$ photoexcitation of the SiH_2^{2+} closed-shell system. Therefore the photoelectron spectrum looks like the photoabsorption spectrum of a closed-shell species. In the difficult analysis of such a spectrum the detailed knowledge of MF effects helps substantially for the assignment of the numerous and sometimes entangled peaks. The overall ordering $^3\Sigma$, $^3\Pi_y$, $^3\Pi_x$, $^1\Pi_y$, $^1\Pi_x$, and $^1\Sigma$ is observed in the photoelectron spectrum, even if slightly disturbed by the quasidegeneracy of nonrelativistic $^3\Pi_x$ and $^1\Pi_y$ binding energies. This ordering reflects the molecular orbital scheme observed in Table IV.

IV. CONCLUSIONS

We performed *ab initio* simulations of L -edge photoelectron spectra of the silicon hydride cations $\text{SiH}^+_{(n=1,2,3)}$. Our approach takes into account both SO and electronic relaxation and correlation effects in a nonperturbative scheme and provides accurate core hole binding energies. This procedure is easy to carry out since only a few ingredients are necessary and since it avoids time consuming Breit-Pauli calculations.

Relevant observations emerged for these species in which MF and SO effects are of the same order of magnitude. The comparison of SiH_3^+ and SiH^+ spectra displays interesting features. Different ordering schemes appear at first sight, ei-

ther a $2 + 1$ scheme for SiH_3^+ or a $1 + 1 + 1$ scheme for SiH^+ . The theoretical analysis reveals that this difference comes from the MF splitting signs of the core hole species, which, in turn, stem from the occupation of the outermost valence orbitals in the ground state. The theoretical analysis reveals also different orderings for the Π and Δ molecular symmetries. Such a different BE ordering should lead, according to the Svensson propensity rule, to different patterns in the consecutive Auger spectra. These latter could be thus analyzed more easily and could reveal the spectral designation of the photoelectron lines.

Beyond the fundamental interest of our results, our paper indicates that L -edge photoelectron spectra are good candidates in plasma source diagnostics. Enhanced chemical activities were actually observed recently in x-ray dissociation regions of stellar objects [35,36], where collisions with the dominant atomic hydrogen species produce abundant molecular hydride species including silicon hydrides. Interpretation of experimental spectra and modeling of physical and chemical properties of these complex astrophysical systems required laboratory measurements of photoabsorption, photoionization, and photodissociation cross sections [37,38]. Silicon hydride cations were recently produced in permanent magnet electron cyclotron resonance ion sources by heating silane (SiH_4) gas with microwave sources [39]. But it was quite difficult to select ionization events taking place from their electronic and vibrational fundamental levels [39–41]. Theoretical investigations able to guide experimental observations remained thus necessary.

APPENDIX A: THEORETICAL ELEMENTS FOR CLOSED-SHELL SYSTEMS

1. Cartesian ${}^2\Lambda_{x,y,z}$ and spectral ${}^2\Lambda_{M_J}$ determinants

$${}^2\Sigma_{\frac{1}{2}} = |2\bar{p}_z^{-1}| = |\dots 2p_0 2p_{+1} 2\bar{p}_{+1} 2p_{-1} 2\bar{p}_{-1} \dots|, \quad (\text{A1})$$

$${}^2\bar{\Pi}_{\frac{1}{2}} = |2p_{-1}^{-1}| = |\dots 2p_0 2\bar{p}_0 2p_{+1} 2\bar{p}_{+1} 2\bar{p}_{-1} \dots|, \quad (\text{A2})$$

$${}^2\Pi_{-\frac{1}{2}} = |2\bar{p}_{+1}^{-1}| = |\dots 2p_0 2\bar{p}_0 2p_{+1} 2p_{-1} 2\bar{p}_{-1} \dots|, \quad (\text{A3})$$

$${}^2\Pi_{\frac{3}{2}} = |2\bar{p}_{-1}^{-1}|, \quad (\text{A4})$$

$${}^2\bar{\Pi}_{-\frac{3}{2}} = |2p_{+1}^{-1}|, \quad (\text{A5})$$

$${}^2\Pi_x = |2\bar{p}_x^{-1}| = |\dots 2p_0 2\bar{p}_0 2p_x 2p_y 2\bar{p}_y \dots|, \quad (\text{A6})$$

$${}^2\bar{\Pi}_y = |2p_y^{-1}| = |\dots 2p_0 2\bar{p}_0 2p_x 2\bar{p}_x 2\bar{p}_y \dots|. \quad (\text{A7})$$

The relations between the Cartesian $2p_{x,y}$ and the spectral $2p_{\pm 1}$ orbitals are chosen as

$$2p_1 = -\frac{1}{\sqrt{2}}(2p_x + i2p_y), \quad (\text{A8})$$

$$2p_{-1} = \frac{1}{\sqrt{2}}(2p_x - i2p_y). \quad (\text{A9})$$

2. Effective Hamiltonians

Because of Kramers degeneracy the 6×6 effective Hamiltonian can be split in two sub- 3×3 matrices. The

corresponding three-dimensional subspaces are driven, respectively, by $\Sigma_{\frac{1}{2}}$ and $\Sigma_{-\frac{1}{2}}$ terms. In the Cartesian representations the two Hamiltonians have the same representation in the bases $\{(2\bar{p}_x)^{-1}, -i(2\bar{p}_y)^{-1}, -(2p_z)^{-1}\}$ and $\{(2p_x)^{-1}, i(2p_y)^{-1}, (2\bar{p}_z)^{-1}\}$. They are written with the convention of a positive value for the SO parameter:

$$H_{\text{CB}} = \begin{pmatrix} E_x & \frac{\gamma}{2} & \frac{\gamma}{2} \\ \frac{\gamma}{2} & E_y & \frac{\gamma}{2} \\ \frac{\gamma}{2} & \frac{\gamma}{2} & E_z \end{pmatrix}. \quad (\text{A10})$$

These matrices are identical to those obtained by Fink and coworkers [13].

The transition towards the spectral basis is made thanks to the combinations $\frac{1}{\sqrt{2}}[(2\bar{p}_x)^{-1} \pm i(2\bar{p}_y)^{-1}]$. Indeed these combinations are, respectively, related to ${}^2\Pi_{-\frac{3}{2}}$ and ${}^2\Pi_{\frac{1}{2}}$ terms. In the spectral (${}^2\Pi_{-\frac{3}{2}}, {}^2\Pi_{\frac{1}{2}}, {}^2\Sigma_{\frac{1}{2}}$) and (${}^2\Pi_{\frac{3}{2}}, {}^2\Pi_{-\frac{1}{2}}, {}^2\Sigma_{-\frac{1}{2}}$) bases the Hamiltonians have the same representation:

$$H_{\text{SB}} = \begin{pmatrix} {}^2\Pi_{-\frac{3}{2}} & {}^2\Pi_{\frac{1}{2}} & {}^2\Sigma_{\frac{1}{2}} \\ \bar{E} - \frac{\gamma}{2} & \Delta & 0 \\ \Delta & \bar{E} + \frac{\gamma}{2} & \frac{\gamma}{\sqrt{2}} \\ 0 & \frac{\gamma}{\sqrt{2}} & E_z \end{pmatrix} \quad (\text{A11})$$

where $\bar{E} = \frac{E_x + E_y}{2}$ and $\Delta = \frac{E_x - E_y}{2}$.

This description has the advantage to show the existence of two block-diagonal submatrices in the case where $\Delta = 0$, that is to say, when the nonrelativistic E_x and E_y energies are degenerate.

APPENDIX B: THEORETICAL ELEMENTS FOR OPEN-SHELL SYSTEMS

1. Antisymmetrized ${}^{2S+1}\Lambda_{M_J}$ spectral and ${}^{2S+1}\Lambda_{x,y,z}^{M_S}$ Cartesian basis sets

The convention for the spectral determinants is derived from the example below:

$$|2p_{-1}^{-1}\sigma_{\text{HO}}| = |\dots 2p_0 2\bar{p}_0 2p_{+1} 2\bar{p}_{+1} 2\bar{p}_{-1} \dots \sigma_{\text{HO}}| \quad (\text{B1})$$

where σ_{HO} is the outermost molecular valence orbital.

The convention for the spectral basis sets is derived from the examples below:

$${}^3\Sigma_{-1} = |2p_z^{-1}\bar{\sigma}_{\text{HO}}|, \quad (\text{B2})$$

$${}^3\Pi_2 = |2\bar{p}_{-1}^{-1}\sigma_{\text{HO}}|, \quad (\text{B3})$$

or from the conventional combinations satisfying the antisymmetrization postulate

$${}^{1,3}\Pi_{\pm 1} = \frac{1}{\sqrt{2}}[\pm |2\bar{p}_{\mp 1}^{-1}\bar{\sigma}_{\text{HO}}| - |2p_{\mp 1}^{-1}\sigma_{\text{HO}}|], \quad (\text{B4})$$

$${}^{1,3}\Sigma_0 = \frac{1}{\sqrt{2}}[\pm |2\bar{p}_0^{-1}\bar{\sigma}_{\text{HO}}| - |2p_0^{-1}\sigma_{\text{HO}}|]. \quad (\text{B5})$$

In the $M_J = 0$ subspace the basis sets corresponding to the two irreducible representations $M_J = 0^+$ and 0^- as defined by Herzberg [34] are chosen:

$${}^3\Pi_{0^\pm} = \frac{1}{\sqrt{2}}[|2p_{-1}^{-1}\bar{\sigma}_{\text{HO}}| \pm |2\bar{p}_{+1}^{-1}\sigma_{\text{HO}}|]. \quad (\text{B6})$$

The Σ_0 terms belong, respectively, to the representations ${}^3\Sigma_{0+}$ and ${}^1\Sigma_{0-}$. Combinations of the ${}^3\Pi_{\pm 2}$ terms, satisfying even and odd character under the $M_J \rightarrow -M_J$ transformation, are introduced:

$${}^3\Pi_{|2|^{\pm}} = \frac{1}{\sqrt{2}}[{}^3\Pi_2 \pm {}^3\Pi_{-2}]. \quad (\text{B7})$$

The convention for the Cartesian determinants is derived from the example below:

$$|2p_x^{-1}\sigma_{\text{HO}}| = |\dots 2p_z 2\bar{p}_z 2\bar{p}_x 2p_y 2\bar{p}_y \dots \sigma_{\text{HO}}|. \quad (\text{B8})$$

The convention for the Cartesian basis sets is derived from the conventional combinations satisfying the antisymmetrization postulate

$${}^{1,3}\Pi_{x,y}^{M_S=0} = \frac{1}{\sqrt{2}}[\pm |2\bar{p}_{x,y}^{-1}\sigma_{\text{HO}}| - |2p_{x,y}^{-1}\sigma_{\text{HO}}|]. \quad (\text{B9})$$

2. Effective 6×6 sub-Hamiltonians in the spectral bases

The Hamiltonians are written with the convention of a positive value for the SO parameter.

In the $|M_J| = 1$ subspace the Hamiltonian is written

$$H_1 = \begin{pmatrix} {}^3\Pi_{-1} & {}^3\Sigma_{-1} & {}^1\Pi_{-1} & {}^3\Pi_1 & {}^3\Sigma_1 & {}^1\Pi_1 \\ \bar{E}_{3\Pi} & \frac{\gamma_{2p}}{2} & \frac{\gamma_{2p}}{2} & \Delta_{3\Pi} & 0 & 0 \\ \frac{\gamma_{2p}}{2} & E_{3\Sigma} & -\frac{\gamma_{2p}}{2} & 0 & 0 & 0 \\ \frac{\gamma_{2p}}{2} & -\frac{\gamma_{2p}}{2} & \bar{E}_{1\Pi} & 0 & 0 & \Delta_{1\Pi} \\ \Delta_{3\Pi} & 0 & 0 & \bar{E}_{3\Pi} & \frac{\gamma_{2p}}{2} & -\frac{\gamma_{2p}}{2} \\ 0 & 0 & 0 & \frac{\gamma_{2p}}{2} & E_{3\Sigma} & \frac{\gamma_{2p}}{2} \\ 0 & 0 & \Delta_{1\Pi} & -\frac{\gamma_{2p}}{2} & \frac{\gamma_{2p}}{2} & \bar{E}_{1\Pi} \end{pmatrix}. \quad (\text{B10})$$

In the $(2^{\pm}, 0^{\pm})$ subspace the 6×6 Hamiltonian is factorized in two 3×3 blocks:

$$H_{02} = \begin{pmatrix} {}^3\Pi_{|2|^+} & {}^3\Pi_{0^+} & {}^3\Sigma_{0^+} & {}^3\Pi_{|2|^-} & {}^3\Pi_{0^-} & {}^1\Sigma_{0^-} \\ \bar{E}_{3\Pi} + \frac{\gamma_{2p}}{2} & \Delta_{3\Pi} & 0 & 0 & 0 & 0 \\ \Delta_{3\Pi} & \bar{E}_{3\Pi} - \frac{\gamma_{2p}}{2} & \frac{\gamma_{2p}}{\sqrt{2}} & 0 & 0 & 0 \\ 0 & \frac{\gamma_{2p}}{\sqrt{2}} & E_{3\Sigma} & 0 & 0 & 0 \\ 0 & 0 & 0 & \bar{E}_{3\Pi} + \frac{\gamma_{2p}}{2} & -\Delta_{3\Pi} & 0 \\ 0 & 0 & 0 & -\Delta_{3\Pi} & \bar{E}_{3\Pi} - \frac{\gamma_{2p}}{2} & -\frac{\gamma_{2p}}{\sqrt{2}} \\ 0 & 0 & 0 & 0 & -\frac{\gamma_{2p}}{\sqrt{2}} & E_{1\Sigma} \end{pmatrix}. \quad (\text{B11})$$

In these matrices $\bar{E}_{3\Pi}$ and $\bar{E}_{1\Pi}$ are the average triplet and singlet energies, respectively, and $\Delta_{3\Pi}$ and $\Delta_{1\Pi}$ are the triplet and singlet energy differences:

$$\bar{E}_{1,3\Pi} = \frac{1}{2}(E_{1,3\Pi_y} + E_{1,3\Pi_x}) \quad (\text{B12})$$

and

$$\Delta_{1,3\Pi} = \frac{1}{2}(E_{1,3\Pi_y} - E_{1,3\Pi_x}). \quad (\text{B13})$$

APPENDIX C: MOLECULAR CHARACTERISTICS

Computed equilibrium distances and vibrational frequencies for SiH_4 and SiH_n^+ ($n = 1-3$) molecules are summarized in Table V. Contrary to the SiH_4 case where significant effects accompanied the formation of a $2p$ core hole, the stretching frequencies and the bond lengths hardly vary in the SiH_3^+ and SiH^+ cases. The creation of a core hole induces thus moderate relaxation effects in these molecules.

TABLE V. Computed equilibrium distances and vibrational frequencies for SiH_4 and SiH_n^+ ($n = 1-3$) molecules. The symmetry of the vibrational mode is given in parentheses. The equilibrium distances are in Å and the vibrational frequencies are in cm^{-1} .

	Ground state					$2p^{-1}$ state				
	$R_e(\text{Å})$	ν_{HSiH}		ν_{SiH}		$R_e(\text{Å})$	ν_{HSiH}		ν_{SiH}	
		Out-of-plane bending	In-plane bending	Symmetric stretching	Antisymmetric stretching		Out-of-plane bending	In-plane bending	Symmetric stretching	Antisymmetric stretching
SiH_4	1.479	924 (T_2)	980 (E)	2236 (A_1)	2240 (T_2)	1.424	979 (T_2)	1096 (E)	2470 (A_1)	2523 (T_2)
SiH_3^+	1.467	836 (A_1)	942 (E)	2269 (A_1)	2349 (E)	1.466	880 (A_1)	956 (E)	2183 (A_1)	2257 (E)
SiH_2^+	1.487		904 (A_1)	2144 (A_1)	2227 (B_2)	1.499		886 (A_1)	2003 (A_1)	2018 (B_2)
SiH^+	1.514				2117 (Σ^+)	1.496				2108 (Σ^+)

- [1] G. M. Bancroft, D. K. Creber, and H. J. Basch, *J. Chem. Phys.* **67**, 4891 (1977).
- [2] J. N. Cutler, G. M. Bancroft, D. G. Sutherland, and K. H. Tan, *Phys. Rev. Lett.* **67**, 1531 (1991).
- [3] J. N. Cutler, G. M. Bancroft, and K. H. Tan, *J. Chem. Phys.* **97**, 7932 (1992).
- [4] L. Karlsson, S. Svensson, P. Baltzer, M. Carlsson-Göthe, M. P. Keane, A. Naves de Brito, N. Correia and B. Wannberg, *J. Phys. B* **22**, 3001 (1989).
- [5] L. Karlsson, S. Svensson, P. Baltzer, A. Naves de Brito, N. Correia, and B. Wannberg, *J. Phys. B* **24**, L589 (1991).
- [6] B. Wannberg, S. Svensson, M. P. Keane, L. Karlsson, and P. Baltzer, *Chem. Phys.* **133**, 281 (1989).
- [7] Z. F. Liu, G. M. Bancroft, K. H. Tan, and M. Schachter, *J. Electron. Spectrosc. Relat. Phenom.* **67**, 299 (1994).
- [8] R. Püttner, M. Domke, K. Schulz, A. Gutiérrez, and G. Kaindl, *J. Phys. B* **28**, 2425 (1995).
- [9] S. Svensson, A. Ausmees, S. J. Osborne, G. Bray, F. Gel'mukhanov, H. Ågren, A. Naves de Brito, O. P. Sairanen, A. Kivimäki, E. Nömmiste, H. Aksela, and S. Aksela, *Phys. Rev. Lett.* **72**, 3021 (1994).
- [10] F. Gel'mukhanov, H. Ågren, S. Svensson, H. Aksela, and S. Aksela, *Phys. Rev. A* **53**, 1379 (1996).
- [11] M. R. F. Siggel, C. Field, L. J. Sæthre, K. J. Børve, and T. D. Thomas, *J. Chem. Phys.* **105**, 9035 (1996).
- [12] H. Aksela, E. Kukk, S. Aksela, O.-P. Sairanen, A. Kivimäki, E. Nömmiste, A. Ausmees, S. J. Osborne, and S. Svensson, *J. Phys. B* **28**, 4259 (1995).
- [13] R. F. Fink, M. Kivilompolo, H. Aksela, and S. Aksela, *Phys. Rev. A* **58**, 1988 (1998).
- [14] R. F. Fink, M. Kivilompolo, and H. Aksela, *J. Chem. Phys.* **111**, 10034 (1999).
- [15] M. Kivilompolo, A. Kivimäki, M. Jurvansuu, H. Aksela, S. Aksela, and R. F. Fink, *J. Phys. B* **33**, L157 (2000).
- [16] J. Palaudoux, T. Kaneyasu, L. Andric, S. Carniato, G. Gamblin, F. Penent, Y. Hikosaka, E. Shigemasa, K. Ito, S. Fritzsche, E. Kukk, S. Sheinerman, R. F. Fink, P. Lablanquie, and R. Püttner, *Phys. Rev. A* **98**, 043406 (2018).
- [17] S. Svensson, A. Naves de Brito, M. P. Keane, N. Correia, and L. Karlsson, *Phys. Rev. A* **43**, 6441 (1991).
- [18] E. Hudson, D. A. Shirley, M. Domke, G. Remmers, and G. Kaindl, *Phys. Rev. A* **49**, 161 (1994).
- [19] K. J. Børve, *Chem. Phys. Lett.* **262**, 801 (1996).
- [20] K. Ellingsen, T. Saue, H. Aksela, and O. Gropen, *Phys. Rev. A* **55**, 2743 (1997).
- [21] W. L. Jolly, K. D. Bomben, and C. J. Eyermann, *At. Data Nucl. Data Tables* **31**, 433 (1984).
- [22] J. D. Bozek, G. M. Bancroft, J. N. Cutler, and K. H. Tan, *Phys. Rev. Lett.* **65**, 2757 (1990).
- [23] M. W. Schmidt, K. K. Baldrige, J. A. Boatz, S. T. Elbert, M. S. Gordon, J. H. Jensen, S. Koseki, N. Matsunaga, K. A. Nguyen, S. Su, T. L. Windus, M. Dupuis, and J. A. Montgomery, *J. Comput. Chem.* **14**, 1347 (1993).
- [24] T. R. Furlani and H. F. King, *J. Chem. Phys.* **82**, 5577 (1985).
- [25] H. F. King and T. R. Furlani, *J. Comput. Chem.* **9**, 771 (1988).
- [26] D. G. Fedorov and M. S. Gordon, *J. Chem. Phys.* **112**, 5611 (2000).
- [27] A. B. Rocha, *J. Mol. Model.* **20**, 2355 (2014).
- [28] N. Kosugi and T. Ishida, *Chem. Phys. Lett.* **329**, 138 (2000).
- [29] A. D. Becke, *J. Chem. Phys.* **98**, 5648 (1993).
- [30] C. Lee, W. Yang, and R. G. Parr, *Phys. Rev. B* **37**, 785 (1988).
- [31] K. A. Peterson and T. H. Dunning, Jr., *J. Chem. Phys.* **117**, 10548 (2002).
- [32] D. E. Woon and T. H. Dunning, Jr., *J. Chem. Phys.* **98**, 1358 (1993).
- [33] J. Ivanic, *J. Chem. Phys.* **119**, 9364 (2003).
- [34] G. Herzberg, *Mol. Spect. and Mol. Struct. Volume I: Spectra of Diatomic Molecules* (Van Nostrand Reinhold, New York, 1950)
- [35] A. O. Benz, S. Bruderer, E. F. Van Dishoeck, P. Staeuber, S. F. Wampfler, M. Melchior, C. Dedes, F. Wyrowski, S. D. Doty, and F. van der Tak, *Astron. Astrophys.* **521**, L35 (2010).
- [36] A. G. G. M. Tielens, *Rev. Mod. Phys.* **85**, 1021 (2013).
- [37] E. Gatuzz, J. García, T. R. Kallman, C. Mendoza, and T. W. Gorczyca, *Astrophys. J.* **800**, 29 (2015).
- [38] W. C. Stolte, V. Jonauskas, D. W. Lindle, M. M. Sant'Anna, and D. W. Savin, *Astrophys. J.* **818**, 149 (2016).
- [39] J.-P. Mosnier, E. T. Kennedy, P. van Kampen, D. Cubaynes, S. Guilbaud, N. Sisourat, A. Puglisi, S. Carniato, and J.-M. Bizau, *Phys. Rev. A* **93**, 061401 (2016).
- [40] E. T. Kennedy, J.-P. Mosnier, P. van Kampen, J.-M. Bizau, D. Cubaynes, S. Guilbaud, S. Carniato, A. Puglisi, and N. Sisourat, *Phys. Rev. A* **97**, 043410 (2018).
- [41] A. Puglisi, N. Sisourat, and S. Carniato, *AIP Conf. Proc.* **1811**, 130002 (2017).